frontiers | Frontiers in Earth Science

TYPE Original Research
PUBLISHED 21 May 2024
DOI 10.3389/feart.2024.1368342

OPEN ACCESS

EDITED BY
Zhaochong Zhang,
China University of Geosciences, China

REVIEWED BY
Dongjie Tang,
China University of Geosciences, China
Qiang Jiang,
China University of Petroleum, Beijing, China

*CORRESPONDENCE
Wei Tian,
davidtian@pku.edu.cn

RECEIVED 10 January 2024
ACCEPTED 29 April 2024
PUBLISHED 21 May 2024

CITATION
Zhang C, Tian W, He Y, Gong M and Li S (2024), The carbon release triggered by 1.32 Ga sill emplacement and its potential environmental implications.
Front. Earth Sci. 12:1368342.
doi: 10.3389/feart.2024.1368342

The carbon release triggered by 1.32 Ga sill emplacement and its potential environmental implications

Chaokun Zhang[1,2], Wei Tian[1,2]*, Yanxin He[1,2], Mingyue Gong[3] and Shun Li[4]

[1]School of Earth and Space Sciences, Peking University, Beijing, China, [2]MOE Key Laboratory of Orogenic Belts and Crustal Evolution, School of Earth and Space Sciences, Peking University, Beijing, China, [3]Sinopec Petroleum Exploration and Development Research Institute, Beijing, China, [4]School of Information Science and Technology, Fudan University, Shanghai, China

Magmatic activity is one of the important pathways for the delivery of deep Earth carbon to the surface. The massive carbon release in this process can have significant impacts on atmospheric-oceanic environment. Previous studies have done a lot of work on the relationship between Phanerozoic magmatic activity and carbon release, but there is relatively limited attention has been given to investigating the association between Precambrian magmatic activity and carbon release. The Yanliao Large Igneous Province at 1.32 Ga exhibits extensive development of sills, and the reaction between sills and surrounding rocks triggers the release of carbon. Simultaneously, the magmatic activity during this period is considered as the final response to the breakup of the Columbia supercontinent, coinciding with the occurrence of the Mesoproterozoic Oxygenation Event To explore the connection between this magmatic activity and global carbon cycling, environmental changes and planetary evolution, nine representative stratigraphic columns are selected from the Yanliao area. We use the SILLi 1.0 1D model by utilizing the one-dimensional finite element method (FEM) to simulate and estimate the amount of carbon release triggered by sill emplacement. The simulation results indicate that the emplacement of sills increased the surrounding rock temperature and vitrinite reflectance, leading to a decrease in the total organic carbon (TOC) content. A large amount of organic carbon and inorganic carbon was released, which was initiated by the reaction between sills and surrounding rocks, with a total carbon release up to 1.24×10^{13} tons. The estimated CO_2 equivalent released during this magma activity episode is expected to be greater than 4.58×10^{13}. In Mesoproterozoic strata, the emplacement of sills activates carbon within the lithosphere could have implications for the global environment. Further work needs to be done in other ancient cratons that possess Lower Riphean strata to find additional evidence of the impact of this magmatic event on the Earth system. From this study, it is evident that magmatic activity during the Precambrian period could promote the activation of carbon in crustal sediments and influence global environment, which can a reference for people to understand the planetary evolution process.

KEYWORDS

sill emplacement, carbon release, environmental effect, precambrian, yanliao area

1 Introduction

In geological history, frequent magmatic activities have occurred, affecting the evolution of the Earth's system. Large Igneous Provinces (LIPs) are large-scale (> 10^5 km^3) mantle-derived magmatic activities dominated by intraplate mafic rocks that occur in a relatively short period of time (<10 Myr) (Ernst, 2014), driving global environmental changes (Wignall, 2001; 2005; Kerr, 2005; Kerr, 2014; Ernst and Youbi, 2017). Large-scale sills are an important component of LIPs. They intrude into the strata and reacts physically and chemically with the surrounding rock, resulting in the release of gases (such as CO_2, CH_4). This leads to significant carbon release and notable environmental effects (Svensen et al., 2004; 2015; Ganino and Arndt, 2009; Svensen et al., 2018a; Heimdal et al., 2018; 2019). Previous researches has extensively reported the relationship between sill emplacement and carbon release during the Phanerozoic eon (Wignall, 2001; 2005; Kerr, 2005; Ernst, 2014; Kerr, 2014; Ernst and Youbi, 2017). Nevertheless, the geological records of the Precambrian period have often been transformed by post-geological processes, which has resulted in poor preservation. As a result, the correlation between sill emplacement and carbon release, as well as planetary environmental changes during Precambrian periods, remains unclear.

With the growing use of numerical simulation methods for both qualitative and quantitative analysis of geological processes, an increasing number of researchers are utilizing these techniques to simulate the intrusion and gas release of sills. This allows for the analysis of the carbon release process and environmental effects that result from sill emplacement (Aarnes et al., 2010; 2011; 2015; Svensen et al., 2015). Such method provides valuable insights into the relationship between Precambrian periods magmatic activities and carbon release, as well as planetary environment.

Located on the northern margin of the North China Craton, a set of large-scale sill has been developed (Ernst, 2014). Building upon a comparative analysis of the geochronology and geochemical characteristics of this set of sill, Zhang et al. (2017a) proposed the concept of the "Yanliao Large Igneous Province" (Yanliao LIP). Evidences from petrology, geochronology, geochemistry, and paleomagnetism suggest the Yanliao LIP exhibits striking similarities to the Derim sills in the McArthur Basin of northern Australia, which is considered to be an unified global LIP (Zhang et al., 2017a). This LIP's peak age is 1,323 Ma and is considered the final response of the craton to the Columbia supercontinent's fragmentation (Zhang et al., 2017b; Cawood, 2020; Zhang et al., 2022b). Mesoproterozoic Oxygenation Event (MOE) is a proposed period of oxygenation during which the global atmosphere-ocean system experienced fluctuations in redox conditions. This hypothesis is supported by the studies of redox-sensitive trace metal (e.g., Mo, U) enrichments and biomarkers preserved in the Xiamaling Formation of North China (Zhang et al., 2016; Diamond et al., 2018; Xu et al., 2024). Taking into account the nearly simultaneous occurrence of the MOE (1.59–1.36 Ga) and the Yanliao LIP (Zhang et al., 2022a). The estimation of the amount of carbon release triggered by this set of sill provides valuable insights into the interplay between magmatic activities, the global carbon cycle and environmental changes of our planet during the Mesoproterozoic era. It contributes to a better understanding of the intricate connections among these factors, shedding light on the Earth's "middle age" phase's planetary evolution.

This study is based on the analysis of nine stratigraphic columns that contain extensive records of large-scale sills from the Yanliao LIP. Using the SILLi 1.0 1D model by utilizing the one-dimensional finite element method, the cooling state of magma and the temperature field of surrounding rocks, as well as the variations in vitrinite reflectance (%Ro) and total organic carbon content (TOC), are finely characterized after the emplacement of the sill. Besides, we inversely estimated the carbon release rate and total release amount associated with the sill emplacement. The accuracy of the model simulations was validated by consistency test with the equivalent vitrinite reflectance (%EqVRo) and total organic carbon content (TOC) measured value of the shales from the sills' intrusion rocks. Our aim was to estimate the carbon release triggered by 1.32 Ga sill emplacement and explore the potential environmental implications of this magmatic activity.

2 Geological setting

Multistage magmatic activity records are found in the Proterozoic strata in Yanliao area, northern margin of North China Craton (Ernst, 2014). Among them, the record of Yanliao LIP is characterized by large-scale (> 1.4×10^5 km^2), short-duration (~1,323 Ma), and have the geochemical characteristics of intraplate magmatic rocks (Zhang et al., 2017a) (Figure 1). Considering the similarities in lithological composition, emplacement age, geochemical characteristics and spatial-temporal distribution indicated by paleomagnetic evidence between the Yanliao Large Igneous Province and the Derim sills (Derim Derim-Galiwinku LIP) in northern Australia (Whelan et al., 2016; Zhang et al., 2017b), it is possible that the scale of this episode of magmatic activity may be even larger (Figure 1B).

The magmatic activity during this period is primarily recorded and preserved in the form of sills. The rocks of this set of sill are mainly diabase (Zhang et al., 2016). The main emplacement is observed within the Xiamaling Formation, while records of this set of sill are also found in the Tieling Formation, Wumishan Formation, and Gaoyuzhuang Formation. The sills primarily intruded into organic-rich shale layers, while others also penetrated into limestone or calcareous graywacke (Shui et al., 2020) (Figure 2). The cumulative thickness of the sills within the formation ranges from 50 m to 1800 m, exhibiting a gradual decrease from the northeast to the southwest. The contact zone between the sill and the surrounding rocks exhibits obvious thermal aureoles. This caused significant hornfelsing and decarbonization of the organic-rich shale (Figures 2A–C) and lead to intense marbleization of the limestone or calcareous graywacke (Figures 2D,E).

3 Samples and methodology

This study was conducted by using the SILLi 1.0 1D model based on nine representative stratigraphic columns containing

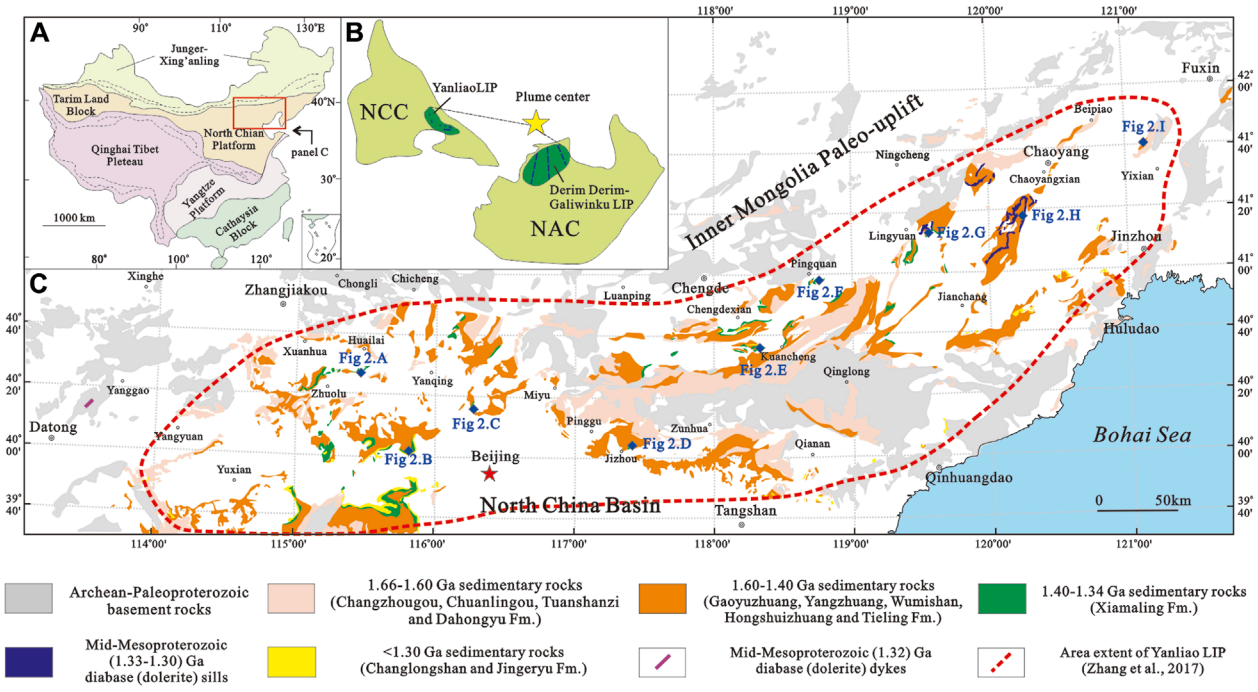

FIGURE 1
The location and areal extent of the 1.32 Ga sills. **(A)** Major tectonic subdivisions of China; **(B)** The reconstruction map of North China-North Australia Craton in 1.32 Ga (modified after Zhang et al., 2017a); **(C)** The sketch map of the Yanliao LIP (modified after Zhang et al., 2017b). Small labeled rhombuses locate the relevant stratigraphic columns in Figure 3.

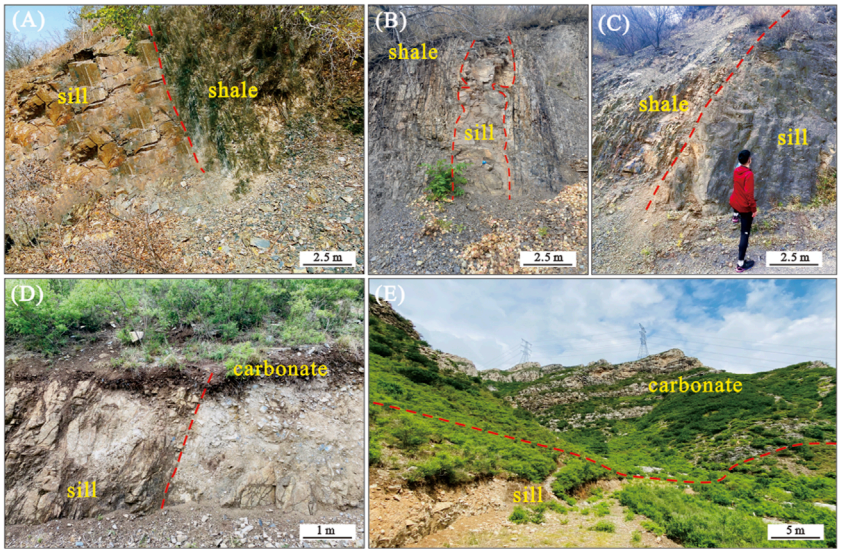

FIGURE 2
Representative outcrop photos of the 1.32 Ga sills. **(A)** Sills emplaced into the Xiamaling Formation in Huailai, Zhangjiakou (N 40°28.7′; E 115°23.4′); **(B)** and **(C)** Sills emplaced into the Xiamaling Formation in Huangtugui, Beijing (N 40°34.5′; E 118°33.3′); **(D)** and **(E)** Sills emplaced into the Wumishan Formation in Chaoyangxian, Chaoyang (N 40°55.7′; E 120°23.6′).

extensive records of sills from the Yanliao LIP (Figure 3). The distribution characteristics of these stratigraphic columns and sill emplacement were referenced from previous research (Zhang et al., 2017a; Deng et al., 2021; Lyu, 2021; Zhang et al., 2022b) and field measurements.

3.1 Samples

The sill samples were collected from the Huailai section (N 40°28.7′; E 115°23.4′), Huangtugui section (N 40°34.5′; E 118°33.3′), Zhenzhuquan section (N 40°33.3′; E 116°21.3′), and Chaoyangxian

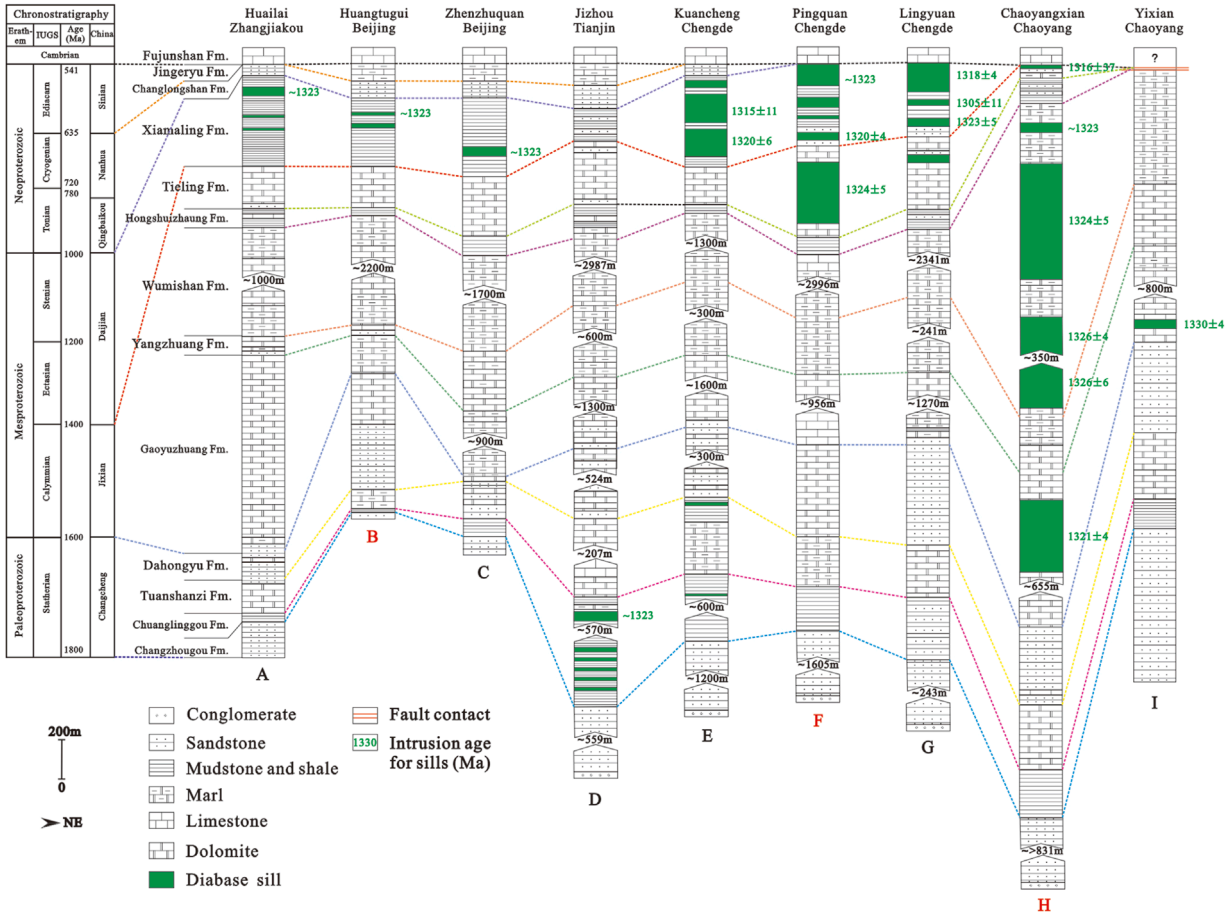

FIGURE 3
Representative stratigraphic columns containing records of sills from the Yanliao LIP (modified after Zhang et al., 2017a). Locations of columns are marked in Figure 1C. Red marks are the stratigraphic column analyzed in Section 4.2.

section (N 40°55.7′; E 120°23.6′). Additionally, nineteen diabase samples were collected for mineralogical analysis from Huailai, Huangtugui, Zhenzhuquan and Chaoyangxian section. Twenty shale samples were collected for equivalent vitrinite reflectance testing and ten samples for TOC analysis from the Huailai section; nineteen shale samples were collected for equivalent vitrinite reflectance testing and ten samples for TOC analysis from the Huangtugui section; and eleven shale samples were collected for equivalent vitrinite reflectance testing and five samples were collected for TOC analysis from the Zhenzhuquan section. The distance of the shale samples to their surrounding rocks can be seem in the Supplementary Tables S1, S2. The weathered surfaces of all samples were cut to ensure that the samples are fresh and free of contamination, then the shale samples were ground to 100 mesh. All the experiments were conducted at the MOE Key Laboratory of Orogenic Belts and Crustal Evolution, School of Earth and Space Sciences, Peking University.

3.2 Petrology analysis

The detailed petrographic analysis of rock thin sections was conducted by the polarizing microscope (Nikon Eclipse LV100NPOL) and the scanning electron microscope (SEM, FEI Quanta 650 FEG) equipped with energy-dispersive X-ray spectroscopy (EDS, Oxford INCA X-Max 50).

To analyze the total organic carbon (TOC) content of shales, the inorganic carbon from 100 mg powdered sediments was removed by treatment with dilute HCl. The resulting residue was then repeatedly washed with deionized water and dried. Analysis of TOC was performed using a Leco CS-230 analyzer. Then, the samples were sectioned either perpendicular or parallel to the bedding and subsequently processed following the guidelines outlined in ISO 7404-2 (2009). Reflectance measurements, in accordance with ISO 7404-5 (2009) and ASTM D7708-14 (2014), were conducted using either the Leica 4500 P microscope with CRAIC microscope photometer or the Leica DM4 M microscope with the Hilgers Technisches Büero Fossil system, equipped with both white and ultraviolet light sources. The equivalent vitrinite reflectance (EqVRo) values were determined using vitrinite-like reflectance (Rv) data, applying the formula established by Luo et al. (2021).

3.3 Carbon release simulation

In this study, we simulated the carbon release from sills by using the SILLi 1.0 1D model established by Iyer et al. (2018) with

the help of the one-dimensional finite element method (FEM). The reliability of this method has been thoroughly validated by previous researchers (Svensen et al., 2018b; Iyer et al., 2018). In this model, each sedimentary layer, including eroded layers, is deposited sequentially in time based on the depositional age. The sedimentation rate of each layer is calculated based on the layer's thickness and the time difference between its top age and the deposition age of the preceding layer (Svensen et al., 2018a). Deposition of an erosional layer occurs in the same way as the layers in the present-day sedimentary column. Sills are emplaced instantaneously at a given time. Based on the geothermal and energy diffusion equations, the temperature changes of each sedimentary layer in the stratigraphic column are calculated under specific boundary temperature conditions. The effective thermal capacity of the rock incorporates the latent heat of fusion associated with the crystallization process occurring within the sill (Aarnes et al., 2010; Iyer et al., 2013). The thermal diffusion equation is modified to incorporate dehydration reactions occurring in the surrounding rocks (Galushkin, 1997; Wang, 2012). The thermal maturity of each sedimentary layer is determined using the EASY%Ro algorithm, which simulates the complex process of kerogen decomposition with increasing temperature based on the Arrhenius equation (Sweeney and Burnham, 1990). Through the aforementioned process, we can obtain the thermal maturity for each stratigraphic horizon. Considering that the studied stratum belongs to the Precambrian period when higher plants had not yet appeared, it is not possible to obtain the vitrinite reflectance (Ro) of organic matter in the formation directly. The simulated vitrinite reflectance values (Ro) represent the equivalent vitrinite reflectance values (EqVRo) of organic matter in the studied strata. The equivalent vitrinite reflectance (EqVRo) values were calculated from vitrinite-like reflectance (Rv) based on the formula reported by Luo et al. (2021): EqVRo=1.07 × Rv-0.18. The release of organic CO_2 is estimated by assessing the TOC variation in the surrounding rocks based on the EASY%Ro method, with its maximum conversion value capped at 85% (Iyer et al., 2018). The release of inorganic CO_2 is estimated by using temperature and pressure curves of carbonate rocks over time, which are pre-calculated using Perplex_X (Connolly and Petrini, 2002). Note that the carbon gas release is calculated as CO_2-equivalents.

4 Results

4.1 Sills petrography

The sill sample have blocky structure, with some parts showing spheroidal weathering (Figure 4A). Under microscopic observation, the sample is identified as diabase with distinct diabasic texture and mineral particles in semi-automorphic granular structure. The main minerals include plagioclase (55–50 vol%), clinopyroxene (30–35 vol%), and amphibole (10–15 vol%). Plagioclase crystallizes earlier than clinopyroxene and exhibits a higher degree of self-shaping. The plagioclase shows slight epidotization alteration along its edges, while the clinopyroxene displays residual structures due to local amphibolization (Figures 4B,C).

4.2 Organic petrology of sill contact zone

At the Huailai section, within a 5.5 m range of the sill contact zone, as the distance increases, the colour of the surrounding rocks transitions from light green to dark gray-black, with an increase in chromaticity; the vitrinite reflectance values of the surrounding rocks decrease from 2.56 to 0.83, with a decrease rate of 67.58%; TOC values increase from 0.20 to 2.00, with an increase rate of 9 (Figure 5A). At the Huangtugui section, within a 3.0 m range of the sill contact zone, as the distance increases, the colour of the surrounding rocks transitions from light yellow to dark gray-black, with an increase in chromaticity; the vitrinite reflectance values of the surrounding rocks decrease from 2.86 to 0.87, with a decrease rate of 69.58%; TOC values increase from 0.03 to 2.45, with an increase rate of 80.67 (Figure 5B). At the Zhenzhuquan section, within a 2.5 m range of the sill contact zone, as the distance increases, the colour of the surrounding rocks transitions from light yellow to dark gray-blue, with an increase in chromaticity; the vitrinite reflectance values of the surrounding rocks decrease from 1.90 to 0.57, with a decrease rate of 70%; TOC values increase from 0.23 to 1.50, with an increase rate of 5.52 (Figure 5C).

4.3 Thermal modelling of carbon release triggered by sills

Input data (Supplementary Tables S3–S11) for the numerical thermal sill model are based on nine stratigraphic columns from the Yanliao LIP (Figure 3). In order to obtain a more conservative estimation, the model utilized an emplacement scenario where individual sills were placed every 10,000 years. If the sills are placed close together, choosing to emplace them simultaneously in the model would cause the aureoles to experience a higher maximum temperature. This could potentially result in an overestimation of the CO_2 production. Pure limestone, despite containing large amounts of CO_2, has a thermal decomposition temperature that surpasses 950°C, exceeding that of impure carbonates (Ganino and Arndt, 2009; Heimdal et al., 2018; Iyer et al., 2018). Given that contact aureoles often cannot attain such high temperatures (Ganino and Arndt, 2009; Supplementary Figure S1), impure carbonates, such as marls, are more inclined to produce substantial volumes of CO_2 during sill emplacement.

Overall, the thermal simulation results indicate that sill emplacement increases the temperature (To ~234°C in average) and vitrinite reflectance (%Ro) (From ~0.50% to ~2.37% in average) of the surrounding rocks, while significantly decreasing its total organic carbon content (TOC) (From ~1.10% to ~0.23% in average) (Supplementary Table S12). By comparing the simulation results with field measured results, at the Huailai section, a 3.0 m thick sill emplacement resulted in a decrease in vitrinite reflectance values of the surrounding rocks from 4.00 to 0.75 within a 5.5 m range, showing a consistency (R^2) of 0.89 with the field measurements; the TOC values within the 5.5 m range of the surrounding rocks increased from 0.00 to 1.11, showing a consistency (R^2) of 0.82 with the field measurements (Figure 5A). At the Huangtugui section, a 0.5 m thick sill emplacement resulted in a decrease in vitrinite reflectance values of the surrounding rocks from 4.00 to 0.70 within a 3.5 m range, showing a consistency (R^2) of 0.85 with

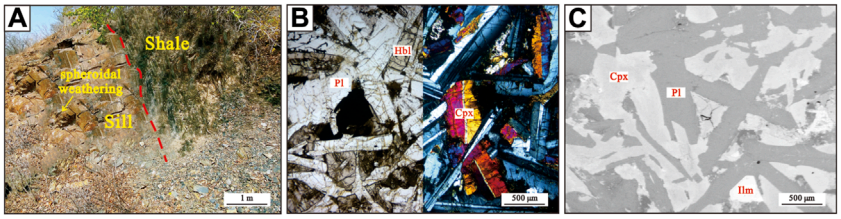

FIGURE 4
The petrography of 1.32Ga sills. **(A)** Field characteristics of sill sample; **(B)** Characteristics of rock thin sections under a polarizing microscope and cross-polarized light microscope; **(C)** Characteristics of rock thin sections under scanning electron microscopy. Pl-plagioclase, Cpx-clinopyroxene, Hbl-hornblende.

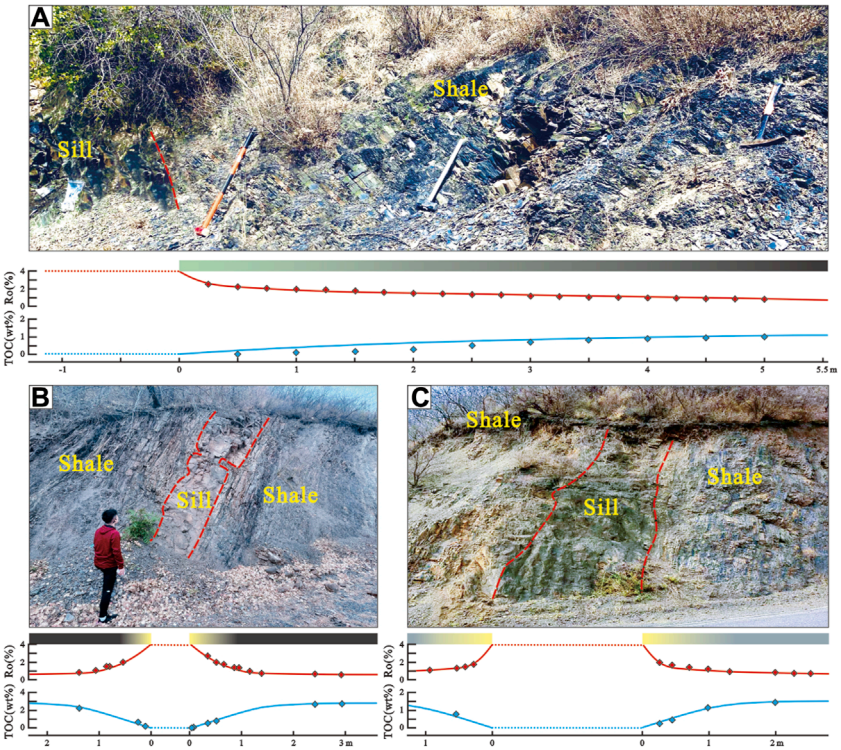

FIGURE 5
The organic petrological characteristics of the surrounding rocks in sill contact zone (Diamond represent measured results, solid lines represent thermal simulation results; **(A)**, Huailai Section; **(B)**, Huangtugui Section; **(C)**, Zhenzhuquan Section).

the field measurements; the TOC values within the 3.5 m range of the surrounding rocks increased from 0.00 to 2.50, showing a consistency (R^2) of 0.91 with the field measurements (Figure 5B). At the Zhenzhuquan section, a 2.5 m thick sill emplacement resulted in a decrease in vitrinite reflectance values of the surrounding rocks from 4.00 to 0.80 within a 2.5 m range, showing a consistency (R^2) of 0.87 with the field measurements; the TOC values within the 2.5 m range of the surrounding rocks increased from 0.00 to 1.50, showing a consistency (R^2) of 0.77 with the field measurements (Figure 5C).

Besides, The peak organic CO_2 flux of this set of sill vary from 4.12 kg/m^2/yr (1,321 Ma) in Chaoyangxian to 4027.78 kg/m^2/yr (1,323 Ma) in Huailai, with an average value of 757.00 kg/m^2/yr. The peak inorganic CO_2 flux of this set of sill vary from 63.70 kg/m^2/yr (1,324 Ma) in Chaoyangxian section to 1,334.46 kg/m^2/yr (1,316 Ma) in the same section, with an average value of 21.64 kg/m^2/yr. The CO_2 production is calculated by subtracting the CO_2 value from background maturation from the peak CO_2 value after sill emplacement (Heimdal et al., 2018). The cumulative organic CO_2 production of this set of sill vary from 0.34 ton/m^2 in Zhenzhuquan section to 1,177.14 ton/m^2 in Chaoyangxian section, with an average value of 143.73 ton/m^2. The cumulative inorganic CO_2 production of this set of sill vary from 1.03 ton/m^2 in Lingyuan section to 58.35 ton/m^2 in Chaoyangxian section, with an average value of 21.64 ton/m^2. The cumulative total CO_2 production of this set of sill vary from 0.34 ton/m^2 in Zhenzhuquan section to 1,235.49 ton/m^2 in Chaoyangxian section, with an average value of 150.94 ton/m^2 (Table 1).

10.3389/feart.2024.1368342

TABLE 1 The carbon release triggered by sill emplacement.

Stratigraphic column	Time (Ma)	Organic CO_2 flux ($kg/m^2/yr$)	Inorganic CO_2 flux ($kg/m^2/yr$)	Organic CO_2 cumulative (ton/m^2)	Inorganic CO_2 cumulative (ton/m^2)	Total CO_2 cumulative (ton/m^2)
Huailai	1,323	4027.78	\	40.51	\	40.51
Huangtugui	1,323	1,576.50	\	10.05	\	10.05
Zhenzhuquan	1,323	7.77	\	0.34	\	0.34
Jizhou	1,323	1744.43	\	12.77	\	12.77
Kuancheng	1,320	675.97	\	24.56	\	24.56
	1,315	451.74	\			
Pingquan	1,324	234.43	211.23	18.46	5.55	24.01
	1,323	1,004.43	\			
Lingyuan	1,323	726.22	639.38	8.80	1.03	9.83
	1,318	491.71	\			
Chaoyangxian	1,326	54.88	844.38	1,177.14	58.35	1,235.49
	1,324	64.05	63.70			
	1,323	\	84.88			
	1,321	4.12	\			
	1,316	245.32	1,334.46			
Yixian	1,330	45.69	\	0.90	\	0.90
AVE		757.00	529.67	143.73	21.64	150.94

Next, we will analyze the thermal effects and cabon release of sill emplacement based on three stratigraphic columns located in the southwest (Huangtugui section), central (Pingquan section), and northeast (Chaoyangxian section) regions of the Yanliao LIP.

4.3.1 Huangtugui section

Stratigraphic column in Huangtugui section comprises 3572.5 m of 13 sedimentary layers and three individual sills (Figure 3). The sill emplacement occurred approximately 1,323 Ma, with intrusion thicknesses of 50 m, 35 m, and 25 m for the three individual sills from bottom to top. The sills are restricted to the Xiamaling Formation, dominated by organic-rich shale.

The modeled thermal effects of each individual sill in stratigraphic column are shown in Figure 5. The temperature rises from background values and reaches a maximum (577°C) at the innermost aureole around each sill. The vitrinite reflectance values (%Ro) increase to a maximum of 4.69%, and correspondingly, the TOC decreases towards each sill to minimum of 01.7%. Only organic CO_2 is generated in aureoles around all of the three sills (Figure 6).

The peak organic CO_2 flux is 1,576.50 $kg/m^2/yr$ in 1,323 Ma. The cumulative CO_2 production for stratigraphic column is 10.05 ton/m^2, which are all organic CO_2 (Figures 7A,B).

4.3.2 Pingquan section

Stratigraphic column Pingquan section comprises 7731 m of 11 sedimentary layers and five individual sills (Figure 3). The sill emplacement occurred in 1,324, 1,323 and 1,320 Ma, with intrusion thicknesses of 360 m, 40 m, 10 m, 40 m and 100 m for the five individual sills from bottom to top. The sills are restricted to the Tieling Formation and Xiamaling Formation, dominated by organic-rich shale and dolomite. The sill emplacement into the sandstone layer at 1,320 Ma, which did not result in carbon release.

The modeled thermal effects of each individual sill in stratigraphic column are shown in Figure 5. The modeled temperature, TOC and vitrinite reflectance values follow the same trend as for stratigraphic column Huangtugui section. The temperature value increase to 792°C, the vitrinite reflectance value (%Ro) increase to 4.68% and the TOC decrease to 0.07%. Both organic CO_2 and organic CO_2 is generated in aureoles around all of the five sills (Figure 6).

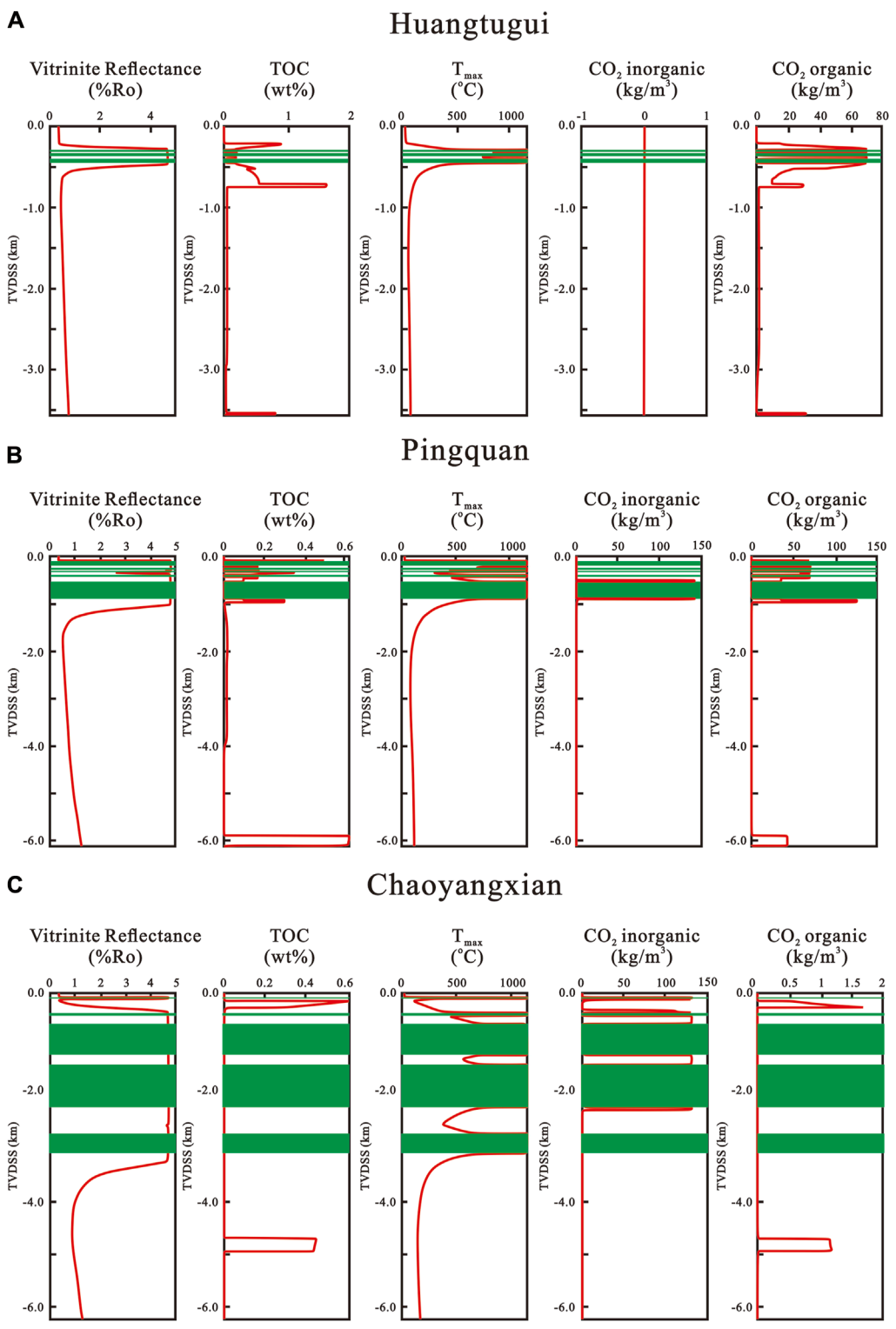

FIGURE 6
Modeled thermal effects of sills emplaced of Yanliao LIP in intervals of 10,000 years, based on the stratigraphic columns of Huangtugui **(A)**, Pingquan **(B)**, Chaoyangxian section **(C)**.

The peak organic CO_2 flux is 234.43 kg/m^2/yr in 1,324 Ma and 1,004.43 kg/m^2/yr in 1,323 Ma. The peak inorganic CO_2 flux is 211.23 kg/m^2/yr in 1,324 Ma. The cumulative CO_2 production for stratigraphic column in 1,324 Ma is 19.88 ton/m^2. The cumulative CO_2 production for stratigraphic column in 1,323 Ma is 4.13 ton/m^2. The total cumulative CO_2 production for stratigraphic column is 24.01 ton/m^2, including 18.46 ton/m^2 organic CO_2 and 5.55 ton/m^2 inorganic CO_2 (Figures 7C,D).

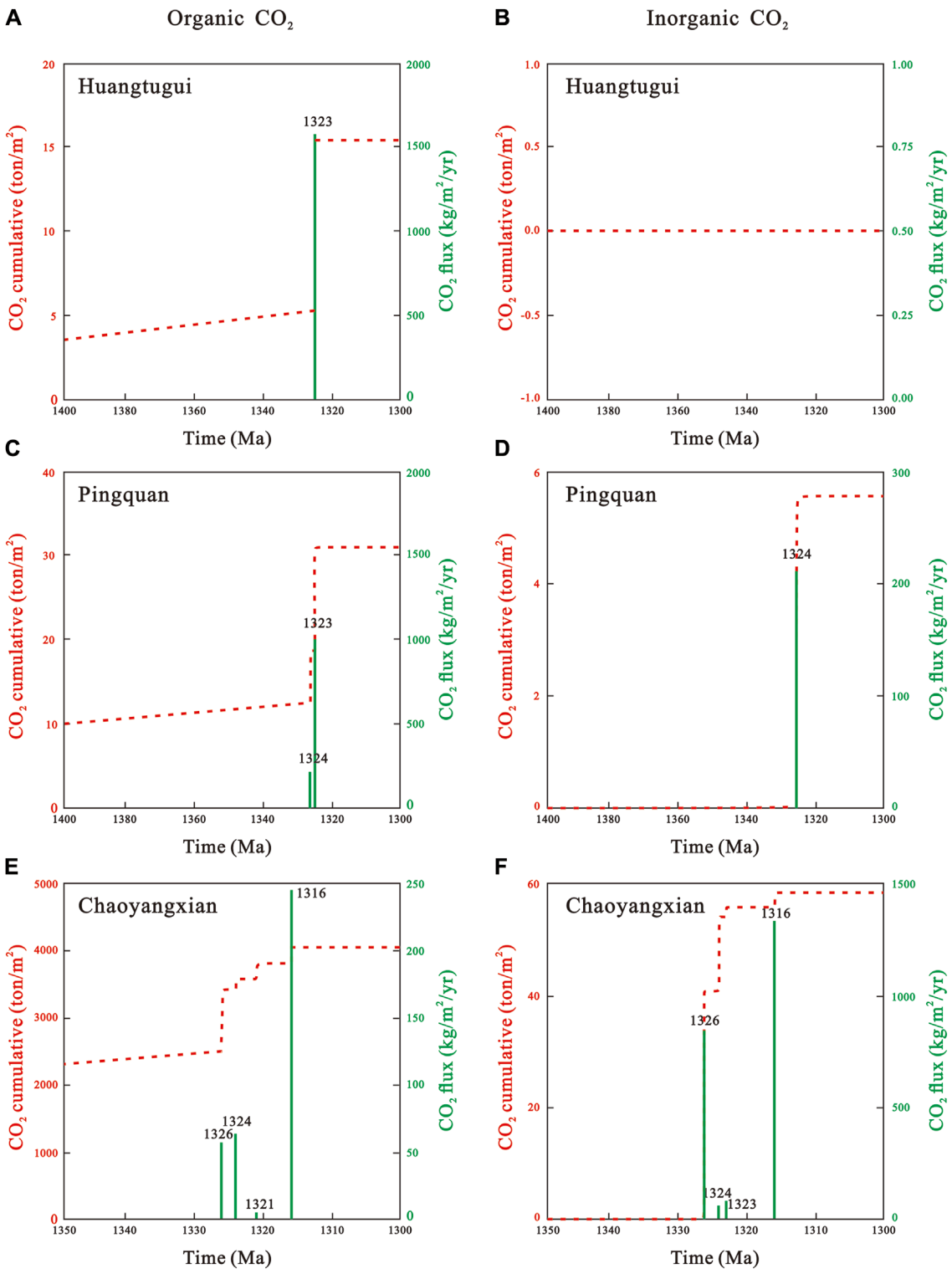

FIGURE 7
Modeled cumulative CO_2 production (red lines) and peak fluxes (green lines) per sill base on the stratigraphic columns of Huangtugui section **(A)**: organic, **(B)**: inorganic, Pingquan section **(C)**: organic, **(D)**: inorganic and Chaoyangxian section **(E)**: organic, **(F)**: inorganic.

4.3.3 Chaoyangxian section

Stratigraphic column Chaoyangxian section comprises 5769.5 m of 10 sedimentary layers and five individual sills (Figure 3). The sill emplacement occurred in 1,326, 1,324, 1,323, 1,321 and 1,316 Ma, with intrusion thicknesses of 366 m, 814 m, 594 m, 54 m and 21 m for the five individual sills from bottom to top. The sills

are restricted to the Gaoyuzhuang Formation, Wumishan Formation and Tieling Formation, dominated by marl and dolomite.

The modeled thermal effects of each individual sill in stratigraphic column are shown in Figure 5. The modeled temperature, TOC and vitrinite reflectance values follow the same trend as for stratigraphic column Huangtugui and Pingquan section. The temperature value increase to 987°C, the vitrinite reflectance value (%Ro) increase to 4.61% and the TOC decrease to 0.10%. Both organic CO_2 and organic CO_2 is generated in aureoles around all of the five sills (Figure 6).

The peak organic CO_2 flux is 54.88 kg/m^2/yr in 1,326 Ma, 64.05 kg/m^2/yr in 1,324 Ma, 4.12 kg/m^2/yr in 1,321 Ma and 245.32 kg/m^2/yr in 1,316 Ma. The peak inorganic CO_2 flux is 844.38 kg/m^2/yr in 1,326 Ma, 63.70 kg/m^2/yr in 1,324 Ma, 84.88 kg/m^2/yr in 1,323 Ma and 1,334.46 kg/m^2/yr in 1,316 Ma. The cumulative CO_2 production for stratigraphic column Chaoyangxian in 1,326 Ma is 929.18 ton/m^2. The cumulative CO_2 production for stratigraphic column in 1,324 Ma is 80.69 ton/m^2. The cumulative CO_2 production for stratigraphic column in 1,323 Ma is 1.23 ton/m^2. The cumulative CO_2 production for stratigraphic column in 1,321 Ma is 157.38 ton/m^2. The cumulative CO_2 production for stratigraphic column in 1,316 Ma is 67.82 ton/m^2. The total cumulative CO_2 production for stratigraphic column is 1,235.49 ton/m^2, including 1,177.14 ton/m^2 organic CO_2 and 58.35 ton/m^2 inorganic CO_2 (Figure 7E,F).

5 Discussion

5.1 Model error analysis

Considering the early formation age of the sill emplacement layers and their subsequent experiences of multiple tectonic transformation, it is challenging to reconstruct the outcrop's exposure and burial history. Taking into account the measured shale in the surrounding rock, which was not affected by the emplacement, with low thermal maturity (EqVRo≤ 0.7%) (Liu et al., 2022), it indicates that the formation emplaced by sills in this area has been in a state of prolonged uplift or shallow burial, thus its burial history after Cambrian period has not been reconstructed. Figure 5 has demonstrated the reliability of the SILLi 1.0D model in simulating the thermal effects of the single-set sill. In order to validate the accuracy of our simulation results of multi-set sills emplacement in study area, we collected equivalent vitrinite reflectance data from 85 sets of sill emplacement surrounding rock samples from Huailai, Huangtugui, Zhenzhuquan and Pingquan section (Liu et al., 2011; Liu et al., 2022 and this study) and TOC data from 38 sets of sill emplacement surrounding rock samples from Huailai, Huangtugui, Zhenzhuquan and Kuancheng section (Shui et al., 2020 and this study) (Supplementary Tables S1 and S2). We analyzed the consistency between the simulated results of our model and the measured results of the samples. The results indicate a high consistency (R^2= 0.94) between the measured equivalent vitrinite reflectance and the simulated vitrinite reflectance (Figure 8A) and a high consistency (R^2= 0.97) between the measured TOC and the simulated TOC (Figure 8B). Prior researches has confirmed the precision of the SILLi 1.0 1D model (Svensen et al., 2018b; Iyer et al., 2018), and its simulated outcomes exhibit a strong consistent with the measured values of relevant indicators. This indicates that the lack of reconstructed burial history after the Cambrian period in this area does not affect the match between model predictions and actual conditions.

5.2 Carbon release and potential environmental effects triggered by sill emplacement

Based on the estimation of SILLi 1.0 1D model on nine typical stratigraphic columns (Figure 9), it was shown that the total cumulative of CO_2 production by sill emplacement into the surrounding rocks was 150.94 ton/m^2. Considering the distribution area of the Derim sill in Northern Australia Craton can reach up to 1.6 × 10^5 km^2 (Kirscher et al., 2021; Mitchell et al., 2021), the total area of this set of sill could reach 3.0×10^5 km^2. The sill emplacement resulted in an equivalent CO_2 release of approximately 4.53 × 10^{13} tons, equivalent to a carbon release of 1.24×10^{13} tons.

When using the 1.8 × 10^6 tons/km^3 CO_2 value for basaltic magma degassing from McCartney et al. (1990), the estimated gas release from volcanic eruptions in this LIP is 5.94 × 10^{11} tons of CO_2 equivalents. The total gas release from this set of magma activity is estimated to be 4.58 × 10^{13} tons of CO_2 equivalents. This is equivalent to 1.53 times (3 × 10^{13} tons) of the CO_2 released by the Siberian Large Igneous Province (Grasby and Bond, 2023), 2.97 times (1.54 × 10^{13} tons) of the CO_2 released by the Central Atlantic Magmatic Province (Schaller et al., 2012), and 21.2 times (2.16 × 10^{12} tons) of the current atmospheric concentration of CO_2 (IPCC, 2013; Jones et al., 2016). It is evident that the carbon release triggered by this set of magma activity is enormous.

In addition to the enormous release of carbon, sill emplacement into the formation can also generate toxic gases such as SO_2 and CH_3Cl through reactions with sulfur-rich, chlorine-rich, and other accessory minerals (such as pyrite) (Shui et al., 2020). The actual gas release during the magma activity period is expected to be greater than our estimated value.

In recent years, there has been considerable debate regarding the ~1.4 Ga oxygenation event (Mesoproterozoic Oxygenation Event, MOE). Nonetheless, mounting evidence now suggests the occurrence of an oxygenation event in both the seawater and atmosphere around 1.4 Ga: (1) Widespread distribution of black shales around 1.4 Ga in North China, North Australia, and potentially in other cratons (Zhang et al., 2018; Diamond et al., 2021), suggesting significant organic matter burial and the subsequent accumulation of high oxygen in the Earth's surface system; (2) The high Mo isotopic values (reaching up to ~1.7‰) found in the shales of the middle Xiamaling Formation are comparable to those of modern seawater (~2.3‰; Diamond et al., 2018), suggesting a more oxygen-rich ocean (Diamond et al., 2018; Diamond and Lyons, 2018; Zhang et al., 2019); (3) Isotope mass balance modeling of U from the northern Australia Craton during the same period suggests that over 75% of the seafloor was probably oxygenated around 1.4 Ga (Yang et al., 2017); (4) The significant negative shift in $\delta^{34}S_{py}$ in the upper Xiamaling Formation is understood as indicating higher seawater sulfate concentration (Wang et al., 2020; Zhang et al., 2022b), potentially attributed to

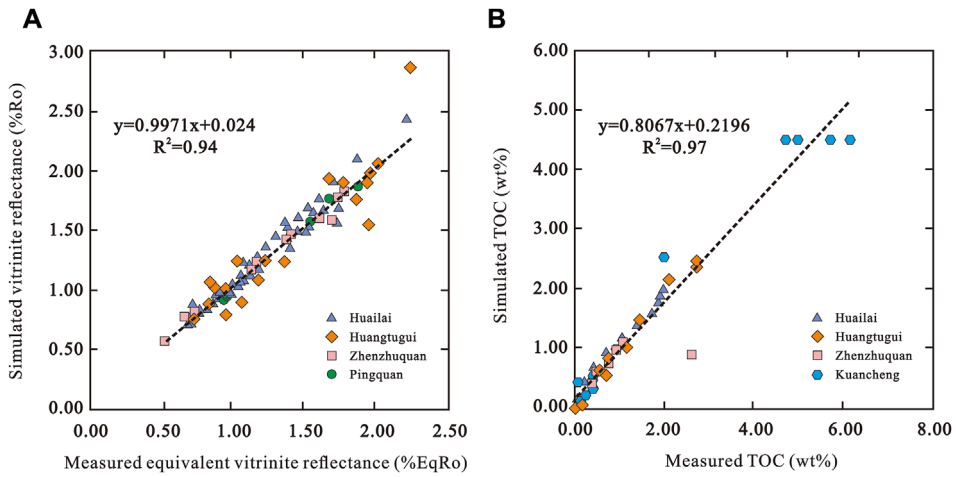

FIGURE 8
Fitting effect of the measured data and simulated results. **(A)** The relationship of measured equivalent vitrinite reflectance and simulated vitrinite reflectance; **(B)** The relationship of measured TOC and simulated TOC.

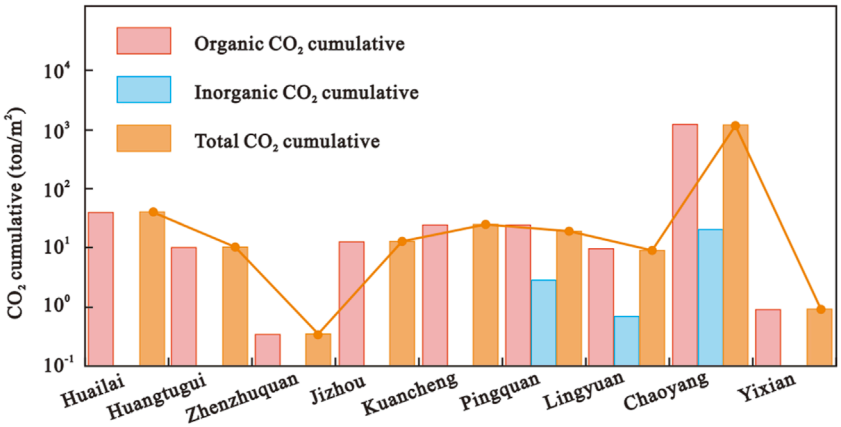

FIGURE 9
The amount of carbon release triggered by ~1.32 Ga sill emplacement in each section.

increased chemical weathering on the continent due to elevated atmospheric O_2 levels (Daines et al., 2017); (5) The Fe speciation and concentrations of redox-sensitive metals in the green shales of the upper Xiamaling Formation similarly indicate oxygenated conditions in the bottom waters, suggesting a rise in marine oxygenation (Zhang et al., 2017b); (6) Elevated I/(Ca + Mg) values in the upper Xiamaling Formation (reaching up to 1.59 μmol/mol), suggesting oxygenated conditions in the surface seawaters. All this evidence suggests that while the oxygenation event ~1.4 Ga may not have been global in scale, it likely represented at least a localized oxygenation event across the Yanliao Area (Xu et al., 2024), which lasting for 230 million years from 1.59 to 1.36 Ga (Zhang et al., 2022a; Figure 10).

The effects of Large Igneous Province (LIP) activity on Earth's surface environment may have been largely consistent across both the Phanerozoic and Precambrian (Ernst and Youbi, 2017). The eruptions of LIPs would release substantial carbon gases into the atmosphere. The magmatism generate volcanic materials (fresh silicate material with high initial reactivity) and expand the surface area accessible for weathering (Jones et al., 2016; Ernst and Youbi, 2017), thereby providing substantial nutrients to the ocean, enhancing primary productivity (Horton, 2015; Diamond et al., 2021; Xu et al., 2024). Based on the positive Hg/TOC excursion, elevated nutrient levels (particularly P) and increased TOC in the middle Xiamaling Formation, Xu et al. (2024) suggested that the weathering of ~1.4–1.35 Ga emplaced LIPs (with a maximum peak at ~1.38 Ga, Zhang et al., 2022b) may have amplified the input of nutrients to the ocean, bolstering higher primary productivity, the burial of organic matter, and ultimately contributing to an oxygenation event (MOE) around 1.4 Ga.

It is worth noting that the ~1.32 Ga sill (Yanliao LIP) and the ~1.4–1.35 Ga LIPs are both attributed to Columbia continental rift system. The Yanliao LIP is specifically identified as the rift zone branch between North Australia and North China, which reached

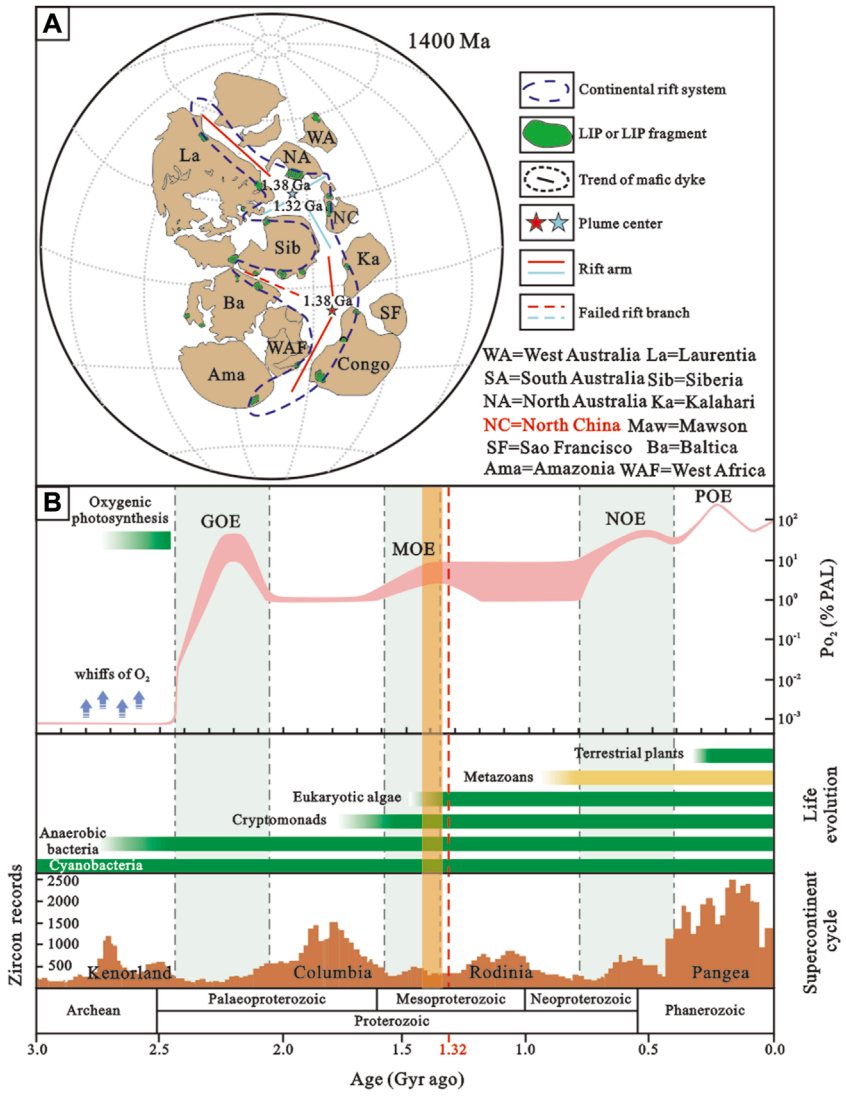

FIGURE 10
The correlation of the oxygenation of Earth's atmosphere, life evolution, supercontinent cycle and the temporal range of sill emplacement (Mesoproterozoic) (modified after Lyons et al., 2014; Canwood, 2020; Zhang et al., 2022b). **(A)** Simplified paleogeographic map of ~1.4 Ga; **(B)** The relationship between Supercontinent Cycles and Planetary Evolution in geological history, the light blue area represents the duration of the oxygenation event; the light orange area represents the dating range of ~1.4–1.35 Ga LIPs; the red dash line represents the average dating of Yanliao LIP (1,323 Ma).

the drifting stage, ultimately leading to the fragmentation and final breakup of Columbia (Zhang et al., 2017a; Wang et al., 2019; Kirscher et al., 2021). Besides, the ~1.32 Ga Yanliao LIP occurred closer in proximity to the North China Craton, which contains records of the MOE event, compared to the occurrence sites of ~1.4–1.35 Ga LIPs (Figure 10A). Considering the calculated release of carbon gas content triggered by the ~1.32 Ga sill emplacement above, it appears that this period of magmatic activity promote the activation of carbon in crustal sediments and may have also impacted the global environment. However, results from previous studies at that time indicate that atmospheric oxygen levels were nearly stable (Zhang et al., 2022a). Therefore, we believe that further discussion is needed on the global climate conditions during the emplacement of the ~1.32 Ga sill. Unfortunately, due to the absence of co-depositional records in the North China Craton and the North Australian Craton during the pre-magmatic period, we lack further evidence to indicate the impact of the ~1.32 Ga sill emplacement on the global ecosystem. Given the occurrence of Lower Riphean sedimentary formations linked to sill emplacement periods in various ancient cratons worldwide (eg. Siberian Craton), it is possible that future exploration of the geological records in these ancient cratons could reveal more information about the environmental impact of the ~1.32 Ga sill emplacement.

5.3 The limitations of simulation results

The application of the SILLi 1.0 1D model to simulate the thermal consequences of sill emplacement offers additional

understanding regarding the release of carbon and environmental ramifications linked to magmatic events (such as Yanliao LIP). However, the thermal simulation results still possess certain limitations: (1) The thermal simulation model is established based on one-dimensional finite element method and cannot simulate the temporal variation of the thermal effects generated by rock intrusion on a three-dimensional level; (2) The model only takes into account the influence of sill emplacement on the vitrinite reflectance (%Ro), total organic carbon content (TOC) and temperature of the surrounding rocks, and does not consider the relationship between other indicators in the formation (such as mineralogical and biomarker indicators) and sill emplacement; (3) The thermal simulation model assumes an approximate maximum conversion rate of 85% for TOC in sedimentary layers, but it does not take into account the complete loss of organic carbon in the contact zone, resulting in an underestimation of released gases. Additionally, the model does not consider the presence of inert kerogens in organic-rich layers, which reduces the amount of organic matter that can be converted into hydrocarbons (Iyer et al., 2017) and affects the transformation rate of TOC; (4) Due to the pre-magmatic activity, the co-depositional records in the North China Craton and the North Australian Craton absent during the sill emplacement. We are currently unable to estimate the amount of released CO_2 that is sequestered in reservoirs as oil and gas, or transformed into calcium carbonate cement in sedimentary rocks without being discharged into the atmosphere. How to overcome the limitations of the SILLi 1.0 1D model and obtain more precise constraints on carbon release estimation and environmental effects assessment caused by sill emplacement is an area worth exploring in future research for us.

6 Conclusion

This study utilizes nine representative stratigraphic columns with records of sill emplacement in the Yanliao LIP in 1.32 Ga. Applying the SILLi 1.0 1D model by one-dimensional finite element method, it conducts simulations and analysis on carbon release and environmental effects triggered by this set of sill emplacement. The model simulation results are subjected to error verification and shortcomings' discussion, leading to the following main conclusions.

(1) The emplacement of the sills results in increase in both the temperature (To 234°C in average) and vitrinite reflectance (To 2.37% in average) of the surrounding rocks, accompanied by a decrease in the total organic carbon content (To 0.23% in average) of the surrounding rocks.
(2) The emplacement of the sill can induce reactions with the surrounding rocks, leading to the release of both organic and inorganic carbon. The estimated total amount of carbon released is approximately 1.24×10^{13} tons. Besides, it is estimated that the CO_2 equivalent released during this period of magma activity will exceed 4.58×10^{13} tons.
(3) The substantial release of gases during the sill emplacement period promote the activation of carbon in crustal sediments and may impact the global environment. Further work need to be done in the sedimentary strata of the Lower Riphean in various ancient cratons globally during the time of the ~1.32 Ga sill emplacement to find evidence of potential environmental impacts caused by this magmatic activity.

Data availability statement

The original contributions presented in the study are included in the article/Supplementary Material, further inquiries can be directed to the corresponding author.

Author contributions

CZ: Data curation, Formal Analysis, Investigation, Methodology, Resources, Software, Validation, Visualization, Writing–original draft, Writing–review and editing. WT: Conceptualization, Funding acquisition, Project administration, Resources, Supervision, Validation, Writing–review and editing. YH: Data curation, Software, Validation, Writing–review and editing. MG: Conceptualization, Investigation, Supervision, Writing–review and editing. SL: Software, Visualization, Writing–review and editing.

Funding

The author(s) declare that financial support was received for the research, authorship, and/or publication of this article. This study was supported by the National Key Research and Development Program of China (2022YFF0800301).

Acknowledgments

We gratefully acknowledge the assistance provided by Prof. Chunjing Wei, Prof. Yang Li, Weipeng Zhu and Bin Wang from School of Earth and Space Sciences of Peking University, Prof. Linhao Fang from College of Geosciences of China University of Petroleum (Beijing) in the verification of model simulation results and language polishing. Besides, We thank the Associate Editor Prof. Zhaochong CZ and three reviewers for their constructive comments that greatly improved the original manuscript.

Conflict of interest

The authors declare that the research was conducted in the absence of any commercial or financial relationships that could be construed as a potential conflict of interest.

Publisher's note

All claims expressed in this article are solely those of the authors and do not necessarily represent those of their

affiliated organizations, or those of the publisher, the editors and the reviewers. Any product that may be evaluated in this article, or claim that may be made by its manufacturer, is not guaranteed or endorsed by the publisher.

Supplementary material

The Supplementary Material for this article can be found online at: https://www.frontiersin.org/articles/10.3389/feart.2024.1368342/full#supplementary-material

References

Aarnes, I., Planke, S., Trulsvik, M., and Svensen, H. (2015). Contact metamorphism and thermogenic gas generation in the Vøring and Møre basins, offshore Norway, during the Paleocene–Eocene thermal maximum. *J. Geol. Soc. Lond.* 172 (5), 588–598. doi:10.1144/jgs2014-098

Aarnes, I., Svensen, H., Connolly, J. A., and Podladchikov, Y. Y. (2010). How contact metamorphism can trigger global climate changes: modeling gas generation around igneous sills in sedimentary basins. *Geochim. Cosmochim. Ac.* 74 (24), 7179–7195. doi:10.1016/j.gca.2010.09.011

Aarnes, I., Svensen, H., Polteau, S., and Planke, S. (2011). Contact metamorphic devolatilization of shales in the Karoo Basin, South Africa, and the effects of multiple sill intrusions. *Chem. Geol.* 281 (3-4), 181–194. doi:10.1016/j.chemgeo.2010.12.007

ASTM D7708-14 (2014). *Standard test method for microscopical determination of theReflectance of vitrinite dispersed in sedimentary rocks*. West Conshohocken, PA: ASTM International. Available at: www.astm.org.

Cawood, P. A. (2020). Earth Matters: a tempo to our planet's evolution. *Geology* 48 (5), 525–526. doi:10.1130/focus052020.1

Connolly, J. A. D., and Petrini, K. (2002). An automated strategy for calculation of phase diagram sections and retrieval of rock properties as a function of physical conditions. *J. Metamorph. Geol.* 20 (7), 697–708. doi:10.1046/j.1525-1314.2002.00398.x

Daines, S. J., Mills, B. J. W., and Lenton, T. M. (2017). Atmospheric oxygen regulation at low Proterozoic levels by incomplete oxidative weathering of sedimentary organic carbon. *Nat. Commun.* 8 (1), 14379. doi:10.1038/ncomms14379

Deng, Y., Wang, H., Lyu, D., Zhang, F., Gao, Z., Ren, R., et al. (2021). Evolution of the 1.8-1.6 Ga Yanliao and xiong'er basins, north China craton. *Precambrian Res.* 365, 106383. doi:10.1016/j.precamres.2021.106383

Diamond, C. W., Ernst, R. E., Zhang, S. H., and Lyons, T. W. (2021). "Breaking the boring billion: a case for solid-Earth processes as drivers of system-scale environmental variability during the mid-Proterozoic," in *Large igneous provinces: a driver of global environmental and biotic changes*, 487–501. doi:10.1002/9781119507444.ch21

Diamond, C. W., and Lyons, T. W. (2018). Mid-Proterozoic redox evolution and the possibility of transient oxygenation events. *Emerg. Top. Life Sci.* 2 (2), 235–245. doi:10.1042/ETLS20170146

Diamond, C. W., Planavsky, N. J., Wang, C., and Lyons, T. W. (2018). What the ~1.4 Ga Xiamaling formation can and cannot tell us about the mid-Proterozoic ocean. *Geobiology* 16 (3), 219–236. doi:10.1111/gbi.12282

Ernst, R. E. (2014). *Large igneous provinces*. Cambridge: Cambridge University Press, 1–653.

Ernst, R. E., and Youbi, N. (2017). How Large Igneous Provinces affect global climate, sometimes cause mass extinctions, and represent natural markers in the geological record. *Palaeogeo, Palaeoclim. Palaeoeco.* 478, 30–52. doi:10.1016/j.palaeo.2017.03.014

Galushkin, Y. I. (1997). Thermal effects of igneous intrusions on maturity of organic matter: a possible mechanism of intrusion. *Org. Geochem.* 26 (11-12), 645–658. doi:10.1016/s0146-6380(97)00030-2

Ganino, C., and Arndt, N. T. (2009). Climate changes caused by degassing of sediments during the emplacement of large igneous provinces. *Geology* 37 (4), 323–326. doi:10.1130/G25325A.1

Grasby, S. E., and Bond, D. P. (2023). How large igneous provinces have killed most life on Earth-numerous times. *Elements* 19 (5), 276–281. doi:10.2138/gselements.19.5.276

Heimdal, T. H., Callegaro, S., Svensen, H. H., Jones, M. T., Pereira, E., and Planke, S. (2019). Evidence for magma–evaporite interactions during the emplacement of the central atlantic magmatic province (CAMP) in Brazil. *Earth Planet. Sci. Lett.* 506, 476–492. doi:10.1016/j.epsl.2018.11.018

Heimdal, T. H., Svensen, H. H., Ramezani, J., Iyer, K., Pereira, E., Rodrigues, R., et al. (2018). Large-scale sill emplacement in Brazil as a trigger for the end-Triassic crisis. *Sci. Rep.* 8 (1), 141. doi:10.1038/s41598-017-18629-8

Horton, F. (2015). Did phosphorus derived from the weathering of large igneous provinces fertilize the Neoproterozoic ocean? *Geochem. Geophy. Geosy.* 16 (6), 1723–1738. doi:10.1002/2015GC005792

IPCC (2013). "Climate change 2013: the physical science basis," in *Contribution of working group I to the fifth assessment report of the intergovernmental panel on climate change*. Editors Stocker, T. F., Qin, D., Plattner, G.-K., Tignor, M., Allen, S. K., Boschung, J., et al. (Cambridge, United Kingdom and New York, NY, USA: Cambridge University Press), 1535.

ISO 7404-2 (2009). *Methods for the petrographic analysis of coals – Part 2: methods of preparing coal samples*. London: International Organization for Standardization. ISO, 1–12. Available at: www.iso.org/standard/42798.html.

ISO 7404-5 (2009). *Methods for the petrographic analysis of coals – Part 5: method of determining microscopically the reflectance of vitrinite*. London: International Organization for Standardization. ISO 7404-5:2009. Available at: www.iso.org/standard/42832.html.

Iyer, K., Rüpke, L., and Galerne, C. Y. (2013). Modeling fluid flow in sedimentary basins with sill intrusions: implications for hydrothermal venting and climate change. *Geochem, Geophys, Geosy.* 14 (12), 5244–5262. doi:10.1002/2013gc005012

Iyer, K., Schmid, D. W., Planke, S., and Millett, J. (2017). Modelling hydrothermal venting in volcanic sedimentary basins: impact on hydrocarbon maturation and paleoclimate. *Earth Planet. Sci. Lett.* 467, 30–42. doi:10.1016/j.epsl.2017.03.023

Iyer, K., Svensen, H. H., and Schimid, D. (2018). SILLi 1.0: a 1D numerical Tool quantifying the thermal effects of sill intrusions. *Geosci. Model Dev.* 11, 43–60. doi:10.5194/gmd-2017-132

Jones, M. T., Jerram, D. A., Svensen, H. H., and Grove, C. (2016). The effects of large igneous provinces on the global carbon and sulphur cycles. *Palaeogeo., Palaeoclim. Palaeoeco.* 441, 4–21. doi:10.1016/j.palaeo.2015.06.042

Kerr, A. C. (2005). Oceanic LIPs: the kiss of death. *Elements* 1 (5), 289–292. doi:10.2113/gselements.1.5.289

Kerr, A. C., Holland, H. D., and Turekian, K. K. (2014). *Treatise on geochemistry, oceanic plateaus. Vol. 4: the crust*. 2. Amsterdam: Elsevier, 631–667.

Kirscher, U., Mitchell, R. N., Liu, Y., Nordsvan, A. R., Cox, G. M., Pisarevsky, S. A., et al. (2021). Paleomagnetic constraints on the duration of the Australia-Laurentia connection in the core of the Nuna supercontinent. *Geology* 49 (2), 174–179. doi:10.1130/G47823.1

Liu, J. L., Zhang, J. C., Wang, S., Chen, L., and Niu, J. L. (2022). Numerical simulation of influence of diabase bed intrusion on thermal evolution of organic rich host rock: a case study of Zhaojiashan Xiamaling Formation. *Pet. Res. Eval. Dev.* 12 (1), 255–264. (in Chinese with English abstract). doi:10.13809/j.cnki.cn32-1825/te.2022.01.022

Liu, Y., Zhong, N. N., Tian, Y. J., Qi, W., and Mu, G. Y. (2011). The oldest oil accumulation in China: Meso-proterozoic Xiamaling Formation bituminous sandstone reservoirs. *Pet. explor. Dev.* 38 (4), 503–512. (in Chinese with English abstract). doi:10.1016/s1876-3804(11)60050-5

Luo, Q., Zhang, L., Zhong, N., Wu, J., Goodarzi, F., Sanei, H., et al. (2021). Thermal evolution behavior of the organic matter and a ray of light on the origin of vitrinitelike maceral in the Mesoproterozoic and Lower Cambrian black shales: insights from artificial maturation. *Int. J. Coal Geol.* 244, 103813. doi:10.1016/j.coal.2021.103813

Lyons, T. W., Reinhard, C. T., and Planavsky, N. J. (2014). The rise of oxygen in Earth's early ocean and atmosphere. *Nature* 506, 307–315. doi:10.1038/nature13068

Lyu, D., Deng, Y., Wang, H., Zhang, F., Ren, R., Gao, Z., et al. (2021). Using cyclostratigraphic evidence to define the unconformity caused by the mesoproterozoic qinyu uplift in the North China craton. *J. Asian Earth Sci.* 206, 104608. doi:10.1016/j.jseaes.2020.104608

McCartney, K., Huffman, A. R., and Tredoux, M. (1990). A paradigm for endogenous causation of mass extinctions. In global catastrophes in Earth history: an interdisciplinary conference on impacts, volcanism, and mass mortality. *Geol. Soc. Am. Spec. Pap.* 247, 125–138. doi:10.13809/j.cnki.cn32-1825/te.2022.01.022

Mitchell, R. N., Kirscher, U., Kunzmann, M., Liu, Y., and Cox, G. M. (2021). Gulf of Nuna: astrochronologic correlation of a Mesoproterozoic oceanic euxinic event. *Geology* 49 (1), 25–29. doi:10.1130/G47587.1

Schaller, M. F., Wright, J. D., Kent, D. V., and Olsen, P. E. (2012). Rapid emplacement of the central atlantic magmatic province as a net sink for CO_2. *Earth Planet. Sci. Lett.* 323, 27–39. doi:10.1016/j.epsl.2011.12.028

Shui, G. H., Zhang, S. H., Hu, G. H., and Zhang, Q. Q. (2020). Estimation of carbon dioxide released during emplacement of ca. 1. 32 Ga mafic sills into the Xiamaling Formation in Yanliao (northern Hebei—western Liaoning) area in the North China Craton and its potential environmental effect. *Geol. Rev.* 66 (4), 939–964. (in Chinese with English abstract). doi:10.16509/j.georeview.2020.04.009

Svensen, H., Fristad, K. E., Polozov, A. G., and Planke, S. (2015). "Volatile generation and release from continental large igneous provinces," in *Volcanism and global environmental change* (Cambridge University Press), 177–192.

Svensen, H., Planke, S., Malthe-Sørenssen, A., Jamtveit, B., Myklebust, R., Rasmussen Eidem, T., et al. (2004). Release of methane from a volcanic basin as a mechanism for initial Eocene global warming. *Nature* 429 (6991), 542–545. doi:10.1038/nature02566

Svensen, H. H., Frolov, S., Akhmanov, G. G., Polozov, A. G., Jerram, D. A., Shiganova, O. V., et al. (2018a). Sills and gas generation in the Siberian. *Traps. philos. T R SOC. A Math. Phys. Eng. Sci.* 376 (2130), 20170080. doi:10.1098/rsta.2017.0080

Svensen, H. H., Polteau, S., Cawthorn, G., and Planke, S. (2018b). "Sub-volcanic intrusions in the Karoo basin, South Africa," in *Physical geology of shallow magmatic systems: dykes, sills and laccoliths* (Cham: Springer), 349–362.

Sweeney, J. J., and Burnham, A. K. (1990). Evaluation of a simple model of vitrinite reflectance based on chemical kinetics. *AAPG Bull.* 74 (10), 1559–1570. doi:10.1306/0c9b251f-1710-11d7-8645000102c1865d

Wang, C., Li, Z.-X., Peng, P., Pisarevsky, S., Liu, Y., Kirscher, U., et al. (2019). Long-lived connection between the North China and North Australian cratons in supercontinent Nuna: paleomagnetic and geological constraints. *Sci. Bull.* 64, 873–876. doi:10.1016/j.scib.2019.04.028

Wang, D. (2012). Comparable study on the effect of errors and uncertainties of heat transfer models on quantitative evaluation of thermal alteration in contact metamorphic aureoles: thermophysical parameters, intrusion mechanism, pore-water volatilization and mathematical equations. *Int. J. Coal Geol.* 95, 12–19. doi:10.1016/j.coal.2012.02.002

Wang, H. Y., Zhang, Z. H., Li, C., Algeo, T. J., Cheng, M., and Wang, W. (2020). Spatiotemporal redox heterogeneity and transient marine shelf oxygenation in the Mesoproterozoic ocean. *Geochim. Cosmochim. Ac.* 270, 201–217. doi:10.1016/j.gca.2019.11.028

Whelan, J. A., Beyer, E. E., Donnellan, N., Bleeker, W., Chamberlin, K. R., Soderlund, U., et al. (2016). "1.4 billion years of Northern Territory geology: insights from collaborative U-Pb zircon and baddeleyite dating," in *Annual geoscience exploration seminar (AGES) proceedings vol. 1* (Australia: Northern Territory Geological Survey Darwin), 116–123.

Wignall, P. B. (2001). Large igneous provinces and mass extinctions. *Earth-science Rev.* 53 (1-2), 1–33. doi:10.1016/s0012-8252(00)00037-4

Wignall, P. B. (2005). The link between large igneous province eruptions and mass extinctions. *Elements* 1 (5), 293–297. doi:10.2113/gselements.1.5.293

Xu, L., Lechte, M., Shi, X., Zheng, W., Zhou, L., Huang, K., et al. (2024). Large igneous province emplacement triggered an oxygenation event at ~1.4 Ga: evidence from mercury and paleo-productivity proxies. *Geophys. Res. Lett.* 51, e2023GL106654. doi:10.1029/2023GL106654

Yang, S., Kendall, B., Lu, X. Z., Zhang, F. F., and Zheng, W. (2017). Uranium isotope compositions of mid-Proterozoic black shales: evidence for an episode of increased ocean oxygenation at 1.36 Ga and evaluation of the effect of post-depositional hydrothermal fluid flow. *Precambrian Res.* 298, 187–201. doi:10.1016/j.precamres.2017.06.016

Zhang, S. C., Wang, H. J., Wang, X. M., and Ye, Y. T. (2022a). Mesoproterozoic oxygenation event. *Sci. China Earth Sci.* 52 (1), 26–52. doi:10.1007/s11430-020-9825-x

Zhang, S. C., Wang, X. M., Wang, H. J., Bjerrum, C. J., Hammarlund, E. U., Costa, M. M., et al. (2016). Sufficient oxygen for animal respiration 1,400 million years ago. *P. Natl. Acad. Sci.* 113 (7), 1731–1736. doi:10.1073/pnas.1523449113

Zhang, S. C., Wang, X. M., Wang, H. J., Bjerrum, C. J., Hammarlund, E. U., Haxen, E. R., et al. (2019). Paleoenvironmental proxies and what the Xiamaling formation tells us about the mid-Proterozoic ocean. *Geobiology* 17 (3), 225–246. doi:10.1111/gbi.12337

Zhang, S. C., Wang, X. M., Wang, H. J., Hammarlund, E. U., Su, J., Wang, Y., et al. (2017a). The oxic degradation of sedimentary organic matter 1400 Ma constrains atmospheric oxygen levels. *Biogeosciences* 14 (8), 2133–2149. doi:10.5194/bg-14-2133-2017

Zhang, S. H., Ernst, R. E., Pei, J. L., Zhao, Y., Zhou, M. F., and Hu, G. H. (2018). A temporal and causal link between ca. 1380 Ma large igneous provinces and black shales: implications for the Mesoproterozoic time scale and paleoenvironment. *Geology* 46 (11), 963–966. doi:10.1130/G45210.1

Zhang, S. H., Ernst, R. E., Yang, Z., Zhou, Z., Pei, J., and Zhao, Y. (2022b). Spatial distribution of 1.4-1.3 Ga LIPs and carbonatite-related REE deposits: evidence for large-scale continental rifting in the Columbia (Nuna) supercontinent. *Earth Planet. Sci. Lett.* 597, 117815. doi:10.1016/j.epsl.2022.117815

Zhang, S. H., Zhao, Y., Li, X. H., Ernst, R. E., and Yang, Z. Y. (2017b). The 1.33-1.30 Ga Yanliao large igneous province in the North China craton: implications for reconstruction of the Nuna (Columbia) supercontinent, and specifically with the North Australian craton. *Earth Planet. Sci. Lett.* 465, 112–125. doi:10.1016/j.epsl.2017.02.034

Zhao, W. Z., Wang, X. M., Hu, S. Y., Zhang, S. C., Wang, H. J., Guan, S. W., et al. (2019). Hydrocarbon generation characteristics and exploration prospects of Proterozoic source rocks in China. *Sci. China Earth Sci.* 49 (6), 909–934. doi:10.1007/s11430-018-9312-4